Supercrystals from Crystallization of Octahedral MnO Nanocrystals

Shuifen Xie, Xi Zhou, Xiguang Han, Qin Kuang,* Mingshang Jin, Yaqi Jiang, Zhaoxiong Xie,* and Lansun Zheng

State Key Laboratory for Physical Chemistry of Solid Surfaces & Department of Chemistry, College of Chemistry and Chemical Engineering, Xiamen University, Xiamen 361005, China

Received: August 7, 2009; Revised Manuscript Received: September 7, 2009

Guided by the concept of regarding nanoparticles as superatoms or supermolecules in colloidal solution, we design a facile crystallization approach for preparation of 3D supercrystals (SCs). Dispersive states of as-prepared MnO nanocrystals (NCs) in solvents of cyclohexane and ethanol were studied to illuminate the effects of solvents. Ethanol was demonstrated to be the most appropriate solvent, and a large amount of microscale cubic SCs built by octahedral MnO NCs was created via direct crystallization. Although two types of packing structures are well-defined, the MnO SCs prefer the one with the higher packing efficiency of 88.89% for minimizing system energy. The crystallization process undergoes a dynamic attachment and exchange mechanism.

1. Introduction

Ordered assembly of nanostructures can create new performance of nanoparticles, such as the tunable plasmonic response and the appearance of the photonic forbidden band in three-dimensional (3D) super-nanostructures.[1−4] Furthermore, the assembly of nanocrystals (NCs) into 3D supercrystals (SCs) is the most promising route for actualizing microdevices involving NCs.[5] Therefore, more and more attention has been recently paid to the ordered assembly of 3D nanostructures.[6−9] Up to date, diversiform bottom-up chemical approaches have been employed for building regular 3D nanostructure assemblies, including the Langmuir−Blodgett technique, matrix confinement, the template-directed approach, substrate engineering, and evaporation-based or magnetizm-induced self-assembly.[1,10−14] A size-/shape-selection post-treatment of NCs, however, is frequently required before the assembly by these approaches because the spontaneous ordered assembly of NCs occurs only with particles confined in a narrow size distribution and a mightily uniform shape.[15] In addition, the shape of the 3D superstructures is uncontrollable, and the nature of the self-assembly behavior of NCs stills remains mysterious. Therefore, it still remains a great challenge to seek more ordinary and convenient methods for the construction of 3D SCs. In this paper, we report a one-step crystallization approach for the preparation of 3D SCs, by which size/shape separation of NCs can be automatically executed.

In a colloidal nanoparticle solution, nanoparticles can be regarded as "superatoms" or "supermolecules". Few researches have also demonstrated that the NCs dispersed in selective solvents behaved as superatoms or supermolecules.[16,17] Therefore, we may assume NCs with a specific size and shape as one kind of homogeneous molecule in colloidal nanoparticle solutions. Those nanoparticles with different sizes and shapes are considered as different molecules. It is well known that the crystallization process is a universal purification route, by which those molecules of the main component in the solution usually crystallize into crystals while those minor components still remain in the solution. On the basis of this concept, one may separate supermolecules in their solution and pack nanoparticles with specific size and shape into 3D SCs by the crystallization.

2. Experimental Section

2.1. Chemicals and Reagents. Manganese acetate ($Mn(OOC_2H_5)_2$), trioctylamine (TOA, 98%), and oleic acid (OA, 90%) were purchased from Alfa Aesar. All reagents were used directly without any further purification.

2.2. Synthesis of Octahedral MnO NCs. Octahedral MnO NCs were synthesized by thermal decomposition of $Mn(OOC_2H_5)_2$ assisted by a mixed organic solvent of TOA and OA. In a typical synthesis, 0.66 mL of OA and 3.0 mL of TOA were mixed in a long test tube (about 40 cm in length and 2.0 cm in diameter) to form a transparent yellowy liquid at room temperature (RT), and then, 0.138 g of $Mn(OOC_2H_5)_2$ was added to the solvent. Then, the bottom of the tube was set on a thermocouple that was in the middle of an erect tubular furnace. Under the control of a program temperature controller, the tubular furnace was heated rapidly to 320 °C in 15 min and kept for 30 min at this temperature. During the process, the initial yellowy mixture changed to a clear orange solution when the temperature reached 320 °C and then gradually turned to green MnO products. The products were cooled naturally to RT in the atmosphere and washed with ethanol or cyclohexane five times with ultrasonic treatment and centrifugation at 10000 r/min for 10 min.

2.3. Fabrication of Cubic MnO SCs. No selective post-treatment was adopted before preparing SCs. The crystallization process of octahedral MnO NCs was actualized by simply dispersing the MnO NCs into anhydrous ethanol using ultrasonication to form a supersaturated solution in a small glass bottle. Then, the solution was sealed and kept static for more than 10 h. Finally, the precipitates in the bottom were collected through a repeated settling separation and dispersed in ethanol for further characterization.

2.4. Characterization and Measurements. The powder X-ray diffraction pattern was recorded using a Panalytical X-pert diffractometer with the copper Kα irradiation. Scanning electron

* To whom correspondence should be addressed. E-mail: zxxie@xmu.edu.cn (Z.X.); qkuang@xmu.edu.cn (Q.K.). Fax: +86-592-2183047. Tel: +86-592-2180627.

10.1021/jp907651d CCC: $40.75
Published on Web 10/08/2009

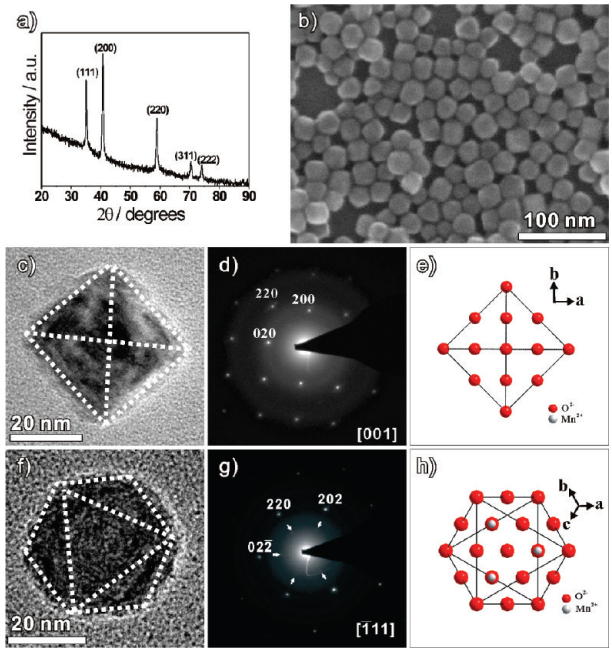

Figure 1. Structure and morphology characterization of as-prepared MnO NCs. (a) XRD pattern of the as-prepared MnO sample. (b) Typical SEM image of dispersive MnO octahedral NCs. (c) TEM image and (d) corresponding SAED pattern of a single MnO octahedron along the [001] axis. (e) Schematic model of the single MnO octahedron projected along the [001] axis. (f) TEM image and (g) corresponding SAED pattern of a single MnO octahedron along the [111] axis. (h) Schematic model of the single MnO octahedron projected along the [111] axis.

microscopy (SEM, Hitachi S-4800) was employed to investigate the morphology and structure of the as-prepared sample. Transmission electron microscopy (TEM) investigations were carried out by using a FEI Tecnai-F30 microscope with an acceleration voltage of 300 kV and a JEM 2100 microscope at 200 kV. The particle size distribution was detected by the dynamic light scattering (DLS) technique (Malvern Nano-ZS).

3. Results and Discussion

To demonstrate this facile crystallization strategy for preparation of highly orientated 3D SCs, octahedral MnO NCs are chosen. Octahedral MnO NCs were synthesized via pyrolysis of manganese acetate assisted by the mixture of OA and TOA, which originates from our previous strategy for the synthesis of ZnO micropyramids.[18] The X-ray diffraction (XRD) pattern (Figure 1a) of the as-prepared sample shows that the product is MnO with cubic rock salt structure (space group: $Fm\bar{3}m$, ICDD 01-075-0626). The morphology of the MnO products was visualized by SEM and TEM. As shown in Figure 1b, the products consist of octahedral nanoparticles with an edge length range approximately from 15 to 30 nm. Although the octahedral shape cannot be well distinguished by the SEM image because of the limitation of the resolution, the TEM images projected from different directions demonstrate that the nanoparticles are of octahedral shape. As shown in Figure 1c−h, the TEM image projected in the [001] direction of a single MnO particle (Figure 1c) is very consistent with an octahedral model projected in the same direction (Figure 1e), and the shape along the [111] direction of the MnO particle (Figure 1f) is the same as that of the corresponding octahedral model (Figure 1h). It should be noted that some inconspicuous additional diffraction spots are sometimes recorded in the SAED patterns as marked by the

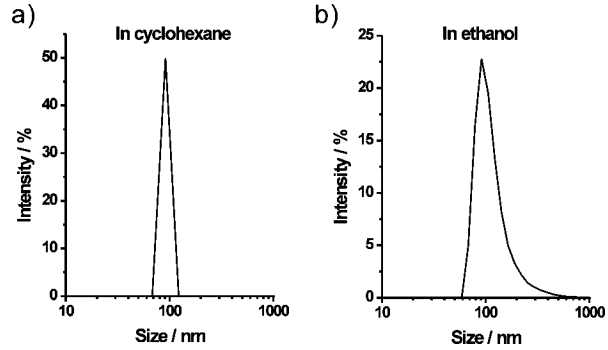

Figure 2. Size distributions of MnO octahedral NCs dispersed in (a) the cyclohexane solvent and (b) the ethanol solvent recorded by the DLS technique.

arrows, which might be attributed to the formation of an ordered Mn vacancy superstructure in MnO[19] or spinel structured Mn_3O_4 on the surface of MnO.[20]

To design the crystallization process of a NC system, the ultimate challenge is to assure the proper solution condition which provides a suitable solubility or mobility of NCs.[21] In other words, the key point is to seek a proper solvent in which NCs have apropos solubility that can provide a dynamic condition for selective crystallization. Since the synthesis process was assisted by the organic solvent, the MnO NCs should adsorb organic solvent and are oleophilic.[22] According to the Law of Similar Mutual Solubility, the as-prepared MnO NCs should be well-dispersed in nonpolar solvents, such as cyclohexane. Dynamic light scattering (DLS) analysis (Figure 2a) indicates that in the diluted cyclohexane solution, octahedral MnO NCs can be well-dispersed, although the apparent particle size (70−130 nm) is much larger than the real ones (15−30 nm) because of the solvation. The result indicates that cyclohexane is not the appropriate solvent for the crystallization of octahedral MnO NCs. Conversely, polar solvents such as ethanol may be better, considering that its high polarity can boost up the hydrophobic interaction among the NCs so as to lower the solubility of NCs in solution. From DLS measurement shown in Figure 2b, it can be found that the size distribution of octahedral MnO NCs in an diluted ethanol solution distinctly has a wider range of several tens to several hundreds of nanometers, which demonstrates that a number of short-range MnO aggregations have been formed in diluted ethanol solution.

According to the above results, we infer that ethanol can provide a required condition for preparing SCs by the crystallization of MnO NCs in our system. Treated as supermolecules, the MnO octahedral NCs were first dispersed in ethanol to form a supersaturated solution using ultrasonication and then kept static for more than 10 h for crystallization. Finally, the products were collected through a repeated settling separation. During the crystallization process, a mass of deposition gradually evolved out on the solution bottom, and the upper solution became more and more limpid, as shown in Figure 3a. The SEM image (Figure 3b) reveals that a large amount of microscale SCs have been gained from crystallization of octahedral MnO NCs. Most of the SCs possess a cube-like morphology (Figure 3c), which amazingly corresponds to the natural crystal symmetry of MnO. To our best knowledge, the SCs with a definite shape (especially nonspherical shapes) are still difficult to obtain, although some successful cases of shape-controlled 3D assembly of NCs has been reported by a number of groups.[23−26] Low-magnification SEM characterization (Figure 3d) indicates that the surfaces are of large terraces at the micrometer scale

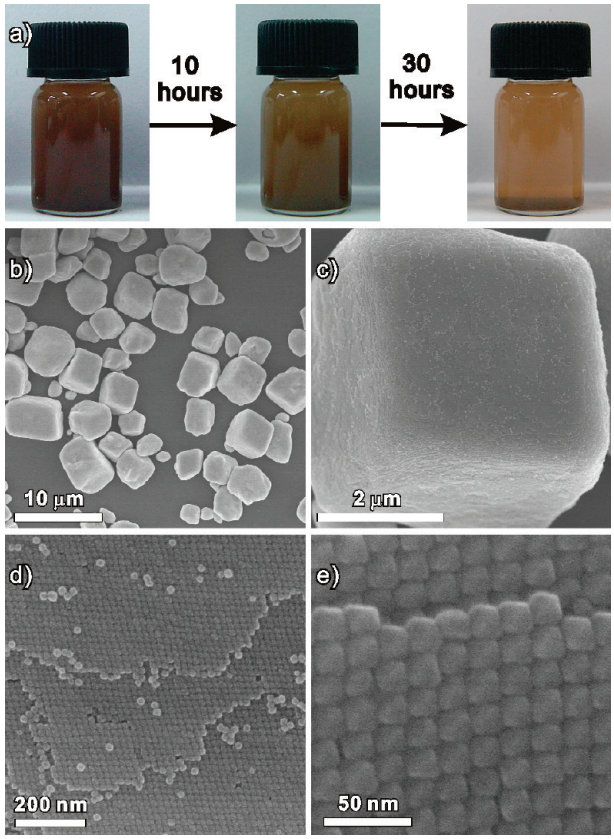

Figure 3. (a) Typical pictures of the crystallization progress. (b) Low-magnification SEM image of the MnO microscale SCs. (c) Typical SEM image of a single MnO SC. (d) Typical SEM image of the surface of a MnO SC and (e) the high-magnification SEM image of the well-oriented organization of MnO octahedral particles on the SCs surface.

consisting of dense-packed NCs. The corresponding further-amplified SEM image (Figure 3e) distinctly gives the packing detail of the octahedral NCs in MnO SCs.

Recently, various 2D and 3D superlattices with highly ordered orientation were observed in the assembly of the Au, In_2O_3, Fe_3O_4, and PbS octahedral NCs.[27−31] Previous studies have demonstrated that there are several packing structures with different packing efficiencies in the octahedral NC assembled superlattices.[27,28] In the present study, two representative types of superlattices were well-identified through detailed analysis. Type-A, only existing in smaller SCs, is presented in Figure 4a. Apparently, octahedral MnO NCs contact each other by their {111} facets to construct closed-packed layers, as shown in the schematic illustration of Figure 4d (see also the Supporting Information for the details). In type-A, the MnO octahedra adhere together in two different ways, the crossed facets share (between two octahedra with the same color in Figure 4d) and complete facets share (between an orange octahedron and a blue one in Figure 4d). As marked by doted lines in Figure 4a and d, the complete facets share of MnO octahedral creates wavelike NC chains along a common [111] direction, and the crossed facets share is applied for joining up the wavelike MnO chains to extend into a plane. Viewing from the direction perpendicular to the complete shared {111} facets, such a 3D configuration of type-A is found to present chains of holes, as shown in the TEM image (Figure 4b) and the corresponding structural model (Figure 4e) projected along the [111] direction. The corresponding selected area electron diffraction (SAED) pattern (Figure 4c) shows a single-crystal feature of the type-A nanoparticle

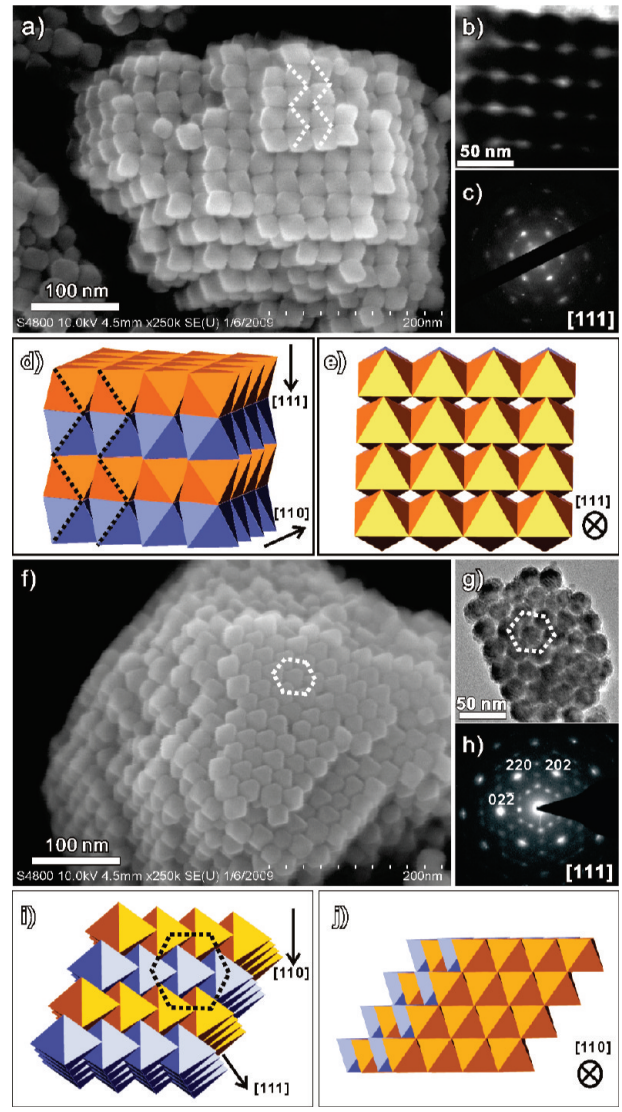

Figure 4. Two representative types of octahedral MnO NC superlattice structures. (a) High-resolution SEM image of type-A SCs. (b) TEM image of type-A SCs viewed along the [111] direction and (c) the corresponding SAED pattern. (d) and (e) Schematic models of type-A projected along the [110] and [111] directions, respectively. (f) High-resolution SEM image of type-B SCs. (g) TEM image of the type-B SCs viewed along the [111] direction and (h) its corresponding SEAD pattern. (i) and (j) Schematic models of type-B SCs projected along the [111] and [110] directions, respectively.

aggregates, demonstrating the formation of SCs. It should be pointed out that subtle orientation inaccuracy could be observed from the elongation of the diffraction spots. In this packing way, the exposed area accounts for 5/8, and the NCs occupancy efficiency is 2/3 = 66.67% (see the details of the calculating process in the Supporting Information), which is similar to the *c*-In_2O_3 superstructures reported in the previous literature.[28] For the type-B, MnO octahedra adopt a hexagonal lattice for the assembly when projecting along the [111] axis, as shown in Figure 4f. In the same monolayer, one octahedron contacts with six other octahedra by the crossed facets share. Three octahedra enclose a cycle to form a trigonal pyramid hole. This hexagonal close-packing arrangement can also be visualized in the corresponding TEM image (Figure 4g) and the schematic illustration of Figure 4i. Figure 4h is a SAED pattern recorded from the direction of the [111] axis, which shows a highly ordered orientation of MnO nanoparticles in the assembled nanoparticle. Figure 4j gives the model viewed along the [110] direction of

type-B superlattices, showing that the upper layer contacts the second layer by crossed facets share. In this configuration, the exposed area of NCs accounts for 4/8, and the packing efficiency marvelously reaches 8/9 = 88.89% (see the details of calculating process in the Supporting Information). As it is widely known, for identical spheres, both the cubic close packing (ccp) and the hexagonal close packing (hcp) offer the highest packing efficiency of only 74.04%,[28,32] which is much lower than that of the type-B packing for octahedral particles. As the type-B packing possesses a higher stacking efficiency and less exposed surface area than those of the type-A packing, the type-B packing is more stable than the type-A packing from the viewpoint of thermodynamics. This viewpoint can well explain that the type-B packing can only be found in the large SCs, as shown in Figure 3e, which is identical with type-B (Figure 4j). This illuminates that, similar to the crystallization of molecules, NCs are spontaneously apt to employ the most stable packing method during the crystallization to minimize the system energy.

Previously, C.A. Mirkin and co-workers have reported the "DNA-programmable nanoparticles crystallization",[33] and "molecule-like behaviors" of NCs have contingently been applied to explain the self-assembly phenomenon.[17,21] Unlike previous evaporation-based approaches, in our system, the MnO octahedra are gradually crystallized out of the supersaturated ethanol solution, which is analogous with the crystallization process in the molecular system. According to the conventional crystallography, accompanied with the crystallization process of SCs, a size-/shape-selection process should spontaneously occurs so as to separate homogeneous molecules or atoms (i.e., NCs with a specific size and shape) from foreign molecules or atoms (i.e., NCs with a different sizes and shapes). As convincing proof, Figure 5a and b shows typical SEM images taken from, respectively, the unassembled NCs left in the solutions after the crystallization process and the assembled SCs settled on the bottom of the solution. From the size distribution histograms (insets of Figure 5a and b) counted over the SEM images, it can be seen that the size distribution is extremely narrow in the assembled SCs, compared to that in the nonassembled NCs. Meanwhile, anisotropic NCs are apt to aggregate with high orientation for minimizing the surface energy. From the SEM image of the stepped surface of SCs (Figure 5c), the intermediate assembly state can be observed at the steps where the particle sizes are not uniform and the orientation is out of order. The results demonstrate that the crystallization process consists of two course, the size selection and orientation adjustment. It should be pointed out that the size-selection and orientation adjustment processes must be dynamic. In other words, the size and orientation of NCs should be selected during the crystallization process by dynamic attachment and exchange (Figure 5d). Otherwise, it is difficult for the formed colloidal nanoparticle clusters to further aggregate into microscale SCs once the periodical packing is blocked by the attachment of size- and orientation-mismatched NCs. Generally, such particle motions as dynamic attachment and exchange are closely related with the force balance between the attraction among the NCs and solvation of individual NCs, which usually depends on the adoptive solvent.[21,34] We speculate that ethanol as the solvent should be appropriate to provide exact force balance for dynamic attachment and exchange in our system of MnO SCs.

4. Conclusion

In summary, on the basis of the concept of regarding nanoparticles as superatoms or supermolecules in colloidal solution, a facile crystallization approach was developed to fabricate highly oriented 3D SCs by selecting a proper solvent. As a successful example, a large amount of microscale cubic 3D SCs was obtained via the crystallization of octahedral MnO NCs in ethanol. The results demonstrate that a size selection and orientation adjustment can be automatically executed when the solvent can provide a dynamic condition for NCs. As a result, our proposed crystallization approach does not require strict demand on the morphological uniformity of initial NCs. This crystallization approach is expected to open a new platform for further design of 3D SCs as well as for various applications in nanoscience and nanotechnology, such as being a general purification route for NCs.

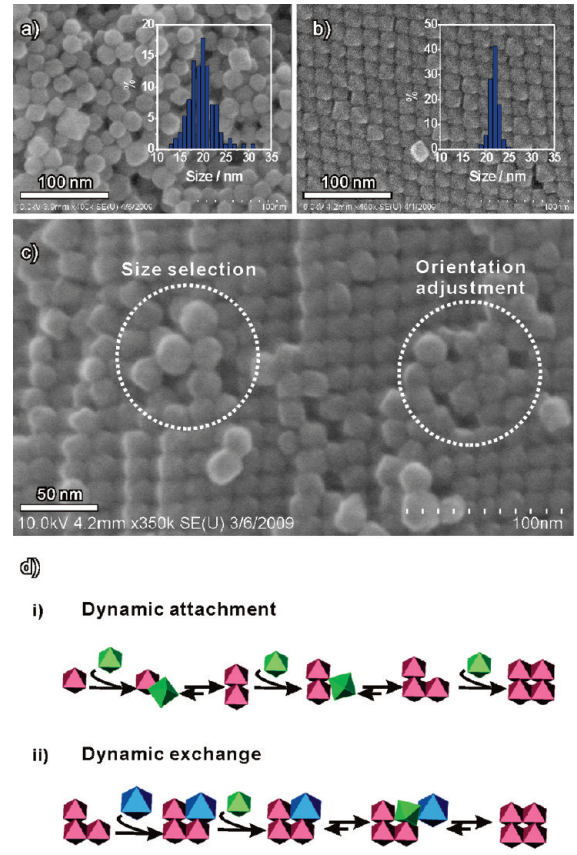

Figure 5. (a) Typical SEM image of unassembled particles left in the solution and the corresponding size distribution histograms. (b) Typical SEM image of an assembled SC and its corresponding size distribution histograms. (c) A SEM image of the stepped surface of the MnO SCs, showing the size selection and orientation adjustment during the crystallization. (d) Scheme of the crystallization process of MnO octahedral nanoparticles; (i) dynamic attachment and (ii) dynamic exchange.

Acknowledgment. This work was supported by the National Natural Science Foundation of China (Grants 20725310, 20721001, 20673085, and 20801045), Key Scientific Project of Fujian Province of China (Grant 2009HZ0002-1), and the National Basic Research Program of China (Grant 2007CB815303 and 2009CB939804).

Supporting Information Available: Schematic illustrations of two facets share modes found in the MnO SCs and the calculating process of the packing efficiency of type-A and type-B. This material is available free of charge via the Internet at http://pubs.acs.org.

References and Notes

(1) Tao, A.; Sinsermsuksakul, P.; Yang, P. D. *Nat. Nanotechnol.* **2007**, *2*, 435–440.

(2) Tao, A. R.; Ceperley, D. P.; Sinsermsuksakul, P.; Neureuther, A. R.; Yang, P. D. *Nano Lett.* **2008**, *8*, 4033–4038.
(3) Ding, T.; Song, K.; Clays, K.; Tung, C. H. *Adv. Mater.* **2009**, *21*, 1936–1940.
(4) Ge, J. P.; Hu, Y. X.; Yin, Y. D. *Angew. Chem., Int. Ed.* **2007**, *46*, 7428–7431.
(5) Parviz, B. A.; Ryan, D.; Whitesides, G. M. *IEEE Trans. Adv. Packag.* **2003**, *26*, 233–241.
(6) Mirkin, C. A.; Letsinger, R. L.; Mucic, R. C.; Storhoff, J. J. *Nature* **1996**, *382*, 607–609.
(7) Redl, F. X.; Cho, K. S.; Murray, C. B.; O'Brien, S. *Nature* **2003**, *423*, 968–971.
(8) Shevchenko, E. V.; Talapin, D. V.; Kotov, N. A.; O'Brien, S.; Murray, C. B. *Nature* **2006**, *439*, 55–59.
(9) Fan, H. Y.; Yang, K.; Boye, D. M.; Sigmon, T.; Malloy, K. J.; Xu, H. F.; López, G. P.; Brinker, C. J. *Science* **2004**, *304*, 567–571.
(10) Fan, H. Y.; Wright, A.; Gabaldon, J.; Rodrguez, A.; Brinker, C. J.; Jiang, Y. B. *Adv. Funct. Mater.* **2006**, *16*, 891–895.
(11) Waterhouse, G. I. N.; Metson, J. B.; Idriss, H.; Sun-Waterhouse, D. X. *Chem. Mater.* **2008**, *20*, 1183–1190.
(12) Xie, R. G.; Liu, X. Y. *J. Am. Chem. Soc.* **2009**, *131*, 4976–4982.
(13) Wang, N.; Guo, L.; He, L.; Cao, X.; Chen, C. P.; Wang, R. M.; Yang, S. H. *Small* **2007**, *3*, 606–610.
(14) Zheng, R. K.; Gu, H. W.; Xu, B.; Fung, K. K.; Zhang, X. X.; Ringer, S. P. *Adv. Mater.* **2006**, *18*, 2418–2421.
(15) Jana, N. R. *Angew. Chem., Int. Ed.* **2004**, *43*, 1536–1540.
(16) Ariga, K.; Hill, J. P.; Lee, M. V.; Vinu, A.; Charvet, R.; Acharya, S. *Sci. Technol. Adv. Mater.* **2008**, *9*, 014109.
(17) Song, Q.; Ding, Y.; Wang, Z. L.; Zhang, Z. J. *J. Phys. Chem. B* **2006**, *110*, 25547–25550.
(18) Zhou, X.; Xie, Z. X.; Jiang, Z. Y.; Kuang, Q.; Zhang, S. H.; Xu, T.; Huang, R. B.; Zheng, L. S. *Chem. Commun.* **2005**, 5572–5574.
(19) Djerdj, I.; Arcon, D.; Jaglicic, Z.; Niederberger, M. *J. Phys. Chem. C* **2007**, *111*, 3614–3623.
(20) Rusakova, I.; Ould-Ely, T.; Hofmann, C.; Prieto-Centurión, D.; Levin, C. S.; Halas, N. J.; Lüttge, A.; Whitmire, K. H. *Chem. Mater.* **2007**, *19*, 1369–1375.
(21) Whitesides, G. M.; Boncheva, M. *Proc. Natl. Acad. Sci. U.S.A.* **2002**, *99*, 4769–4774.
(22) Zhong, X. H.; Xie, R. G.; Sun, L. T.; Lieberwirth, I.; Knoll, W. *J. Phys. Chem. B.* **2006**, *110*, 2–4.
(23) Boal, A. K.; IIhan, F.; DeRouchey, J. E.; Thurn-Albrecht, T.; Russell, T. P.; Rotello, V. M. *Nature* **2000**, *404*, 746–748.
(24) Zhuang, J. Q.; Wu, H. M.; Yang, Y. G.; Cao, Y. C. *Angew. Chem., Int. Ed.* **2008**, *47*, 2208–2212.
(25) Kuchibhatla, S. V. N. T.; Karakoti, A. S.; Sayle, D. C.; Heinrich, H.; Seal, S. *Cryst. Growth Des.* **2009**, *9*, 1614–1620.
(26) Sayle, D. C.; Seal, S.; Wang, Z.; Mangili, B. C.; Price, D. W.; Karakoti, A. S.; Kuchibhatla, S. V. T. N.; Hao, Q.; Mobus, G.; Xu, X.; Sayle, T. X. T. *ACS Nano* **2008**, *2*, 1237–1251.
(27) Chang, C. C.; Wu, H. L.; Kuo, C. H.; Huang, M. H. *Chem. Mater.* **2008**, *20*, 7570–7574.
(28) Lu, W. G.; Liu, Q. S.; Sun, Z. Y.; He, J. B.; Ezeolu, C.; Fang, J. Y. *J. Am. Chem. Soc.* **2008**, *130*, 6983–6991.
(29) Wang, N.; Cao, X.; Guo, L.; Yang, S. H.; Wu, Z. Y. *ACS Nano* **2008**, *2*, 184–190.
(30) Jiang, S. Y.; Xing, S. X.; Wang, Y. F.; Hu, H. L.; Zhao, B.; Zhao, C. *Mater. Lett.* **2008**, *62*, 977–979.
(31) Zhang, L. H.; Wu, J. J.; Liao, H. B.; Hou, Y. L.; Gao, S. *Chem. Commun.* **2009**, 4378–4380.
(32) Zhang, J.; Kumbhar, A.; He, J. B.; Das, N. C.; Yang, K. K.; Wang, J. Q.; Wang, H.; Stokes, K. L.; Fang, J. Y. *J. Am. Chem. Soc.* **2008**, *130*, 15203–15209.
(33) Park, S. Y.; Lytton-Jean, A. K. R.; Lee, B.; Weigang, S.; Schatz, G. C.; Mirkin, C. A. *Nature* **2008**, *451*, 553–556.
(34) Whitesides, G. M.; Grzybowski, B. *Science* **2002**, *295*, 2418–2421.

JP907651D